

Different Energetics at Donor:Acceptor Interfaces in Bilayer and Bulk-Heterojunction Polymer:Non-Fullerene Organic Solar Cells

Yahui Tang, Wen Liang Tan, Zhuping Fei, Martin Heeney, and Christopher R. McNeill*

To understand the limitations placed on the open-circuit voltage of bulk heterojunction (BHJ) organic solar cells, the energy levels of neat donor and acceptor samples are often characterized and applied to study BHJ blends. However, energy levels derived from neat samples may not necessarily reflect those at the donor:acceptor interface in blends. The properties of organic semiconductors are sensitive to microstructural changes, with non-fullerene acceptors (NFAs) in particular known to exhibit different thin-film polymorphs. To investigate the influence of differences in molecular packing in neat and blend films, temperature-dependent current–voltage characteristics are measured for bilayer (BL) and BHJ devices. Herein, the fullerene acceptor PC₇₁BM is compared—whose energy levels are expected to be less sensitive to molecular packing—with the NFA ITIC, paired with the same donor polymer PTB7-Th. It is found that the interfacial energy levels differ for BL and BHJ devices for the PTB7-Th:ITIC system but remain the same for the PTB7-Th:PC₇₁BM system. Furthermore, X-ray scattering measurements identify that ITIC exhibits a different packing mode in neat films and in BHJ blends. Such microstructure-dependent differences between neat and blend samples need to be considered when studying energy losses in NFA BHJ solar cells.

1. Introduction

Numerous investigations have been implemented in recent years on the relationship between the energetic offset at the donor:acceptor (D:A) interface and the efficiency of charge photogeneration in solution-processed bulk heterojunction (BHJ) organic solar cells (OSCs).^[1–8] In many of these studies, the energy levels measured using neat donor/acceptor films are used directly for calculating the energetic offsets in blend films.^[1,8,9] Specifically, the energy of the lowest unoccupied molecular orbital (E_{LUMO}) of neat materials is measured by inverse photoemission spectroscopy (IPES), and the energy of the highest occupied molecular orbital (E_{HOMO}) of neat materials is measured by ultraviolet photoelectron spectroscopy (UPS).^[9–12] The energetic offsets of blends calculated following this approach are based on the assumption that energy levels do not change from neat to blend films, which may lead to contradictory conclusions for devices based on the same D:A blends.^[13,14]


The energetic offsets at the D:A interfaces are critical for the solar cell operations for two reasons. First, the values of lowest unoccupied molecular orbital (LUMO) (or highest occupied molecular orbital (HOMO) offset for hole transfer) are often considered as a “driving force” for charge separation in many studies, and the debate on whether a large driving force is required for efficient charge generation has not yet settled. While it is widely observed for OSCs comprising fullerene acceptors that an energy offset large than 0.3 eV is required for efficient charge separation,^[15,16] a wide range of non-fullerene acceptor (NFA)-based OSCs with apparent small energetic offset have been shown to exhibit efficient charge generation.^[6–8,17] However, it is also argued that a ≈ 0.4 eV LUMO offset is required for achieving efficient charge generation, even for NFAs.^[9] Second, the values of $E_{\text{LUMO,acceptor}} - E_{\text{HOMO,donor}}$ are also important, because they are often used as the effective bandgap energy in the drift-diffusion simulations for BHJ devices based on the metal–insulator–metal framework where the BHJ layer is effectively considered as one material.^[18]

While the measurement of HOMO/LUMO energies of neat materials using UPS/IPES are well established, the calculation

Y. Tang, W. L. Tan, C. R. McNeill
Department of Materials Science and Engineering
Monash University
Clayton, Victoria 3800, Australia
E-mail: christopher.mcneill@monash.edu

Z. Fei
Institute of Molecular Plus
Tianjin Key Laboratory of Molecular Optoelectronic Science
Tianjin University
Tianjin 300072, China

M. Heeney
Department of Chemistry and Centre for Processable Electronics
Imperial College London
London SW7 2AZ, UK

 The ORCID identification number(s) for the author(s) of this article can be found under <https://doi.org/10.1002/solr.202300471>.

© 2023 The Authors. Solar RRL published by Wiley-VCH GmbH. This is an open access article under the terms of the Creative Commons Attribution-NonCommercial License, which permits use, distribution and reproduction in any medium, provided the original work is properly cited and is not used for commercial purposes.

DOI: 10.1002/solr.202300471

of energetic offsets of D:A blends via measuring the neat films is based on the assumption that the energy levels of materials in blends remain the same as the neat films, which may not be true for all materials. This is more problematic in NFA-based systems due to their anisotropic nature and more complex morphological behaviors.^[19,20] It has been reported that the favorable properties of NFAs such as ITIC and Y6 are related to the unique way that these molecules pack in thin films.^[20,21] NFAs such as ITIC and its derivatives have been reported to have different polymorphs in their neat film if processed under different conditions, and the electrical properties of these polymorphs have also been found to differ significantly.^[22] Thus, the LUMO measured of a neat NFA layer may be different to the effective LUMO of an NFA molecule at a donor/acceptor interface inside a BHJ film due to differences in molecular packing/conformation. Previous studies on donor materials such as P3HT have also shown that the HOMO measured of a neat film can depend on the molecular orientation of the film (i.e., face-on vs edge-on) and that these changes correlate with changes in the open-circuit voltage (V_{OC}) of bilayer (BL) solar cells using PCBM as the acceptor.^[23] Therefore, blindly using HOMO/LUMO values derived from neat materials to simulate BHJ devices may lead to misinterpretation of other parameters that describe the dynamics of the recombination/generation processes, for example, the Langevin reduction factor. Because of these reasons, it is worth questioning whether the molecular packing of NFAs changes when blended with a donor material, and whether it induces an energy-level change in blend films compared to neat films that is significant enough to affect the V_{OC} of OSCs.

Temperature-dependent measurements of current density–voltage (J – V) characteristics can provide important insight into the operation of OSCs. By conducting a side-by-side analysis of BHJ and planar BL devices, the effect of potential changes in energy-level alignment at the D:A interface can be investigated. The analytical expression of V_{OC} derived from the Shockley equation for a solar cell with ideality factor n is given by

$$V_{OC} = \frac{nk_B T}{q} \ln \left(\frac{J_{SC}}{J_0} + 1 \right) \quad (1)$$

Such an expression can be expanded to link V_{OC} to the opto-electrical properties of materials via the formula^[24,25]

$$V_{OC} = \frac{E_{CT}}{q} + \frac{k_B T}{q} \ln \left(\frac{J_{SC} h^3 c^2}{f q 2 \pi (E_{CT} - \lambda)} \right) + \frac{k_B T}{q} \ln (EQE_{EL}) \quad (2)$$

where f is the electronic coupling, λ is the reorganization energy of the charge transfer (CT) state absorption process, EQE_{EL} is the external quantum efficiency (EQE) of electroluminescence (EL), and J_{SC} is the short-circuit current density (J_{SC}) of the devices. The second term of Equation (2) represents the radiative recombination energy loss, and the third term represents the non-radiative loss.^[15] Furthermore, based on this equation, the value of qV_{OC} is expected to approach E_{CT} when the temperature approaches 0 K as the second and third terms vanish. Therefore, the linear extrapolation of V_{OC} to 0 K, which is termed as V_{OC}^0 , is expected to be equal to the value of E_{CT}^0 , the value of E_{CT} at 0 K. Such a relationship between V_{OC}^0 and E_{CT}^0 has been

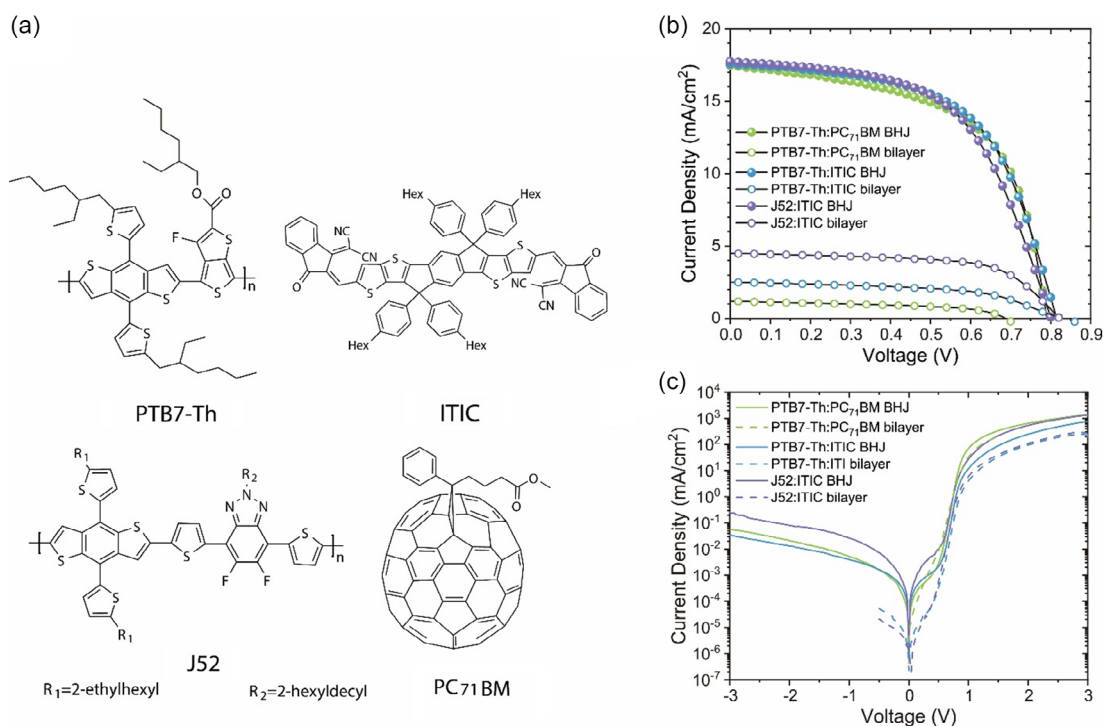


Figure 1. a) Chemical structures of the materials used. b) Current density–voltage (J – V) characteristics of inverted bulk heterojunction (BHJ) solar cells with various donors and acceptors measured under 100 mW cm^{-2} AM 1.5G solar irradiation at room temperature. c) J – V characteristics of inverted BHJ solar cells with various donors and acceptors measured in the dark at room temperature.

Table 1. Photovoltaic parameters of inverted BHJ devices under standard AM 1.5 G solar illumination.

Material donor:acceptor	J_{SC} [mA cm^{-2}]	V_{OC} [V]	Fill factor [%]	PCE [%]
PTB7-Th:PC ₇₁ BM BHJ	17.5	0.79	59	8.1
PTB7-Th/PC ₇₁ BM bilayer	1.2	0.68	51	0.8
PTB7-Th:ITIC BHJ	18.1	0.82	59	8.7
PTB7-Th/ITIC bilayer	2.5	0.85	53	2.1
J52:ITIC BHJ	18.3	0.80	59	8.7
J52/ITIC bilayer	4.5	0.83	62	3.7

demonstrated in thermally evaporated planar heterojunction OSCs and solution-processed BHJ polymer:fullerene OSCs.^[24,26] Although the drift/diffusion lengths of the charge carriers from the D:A interfaces to the electrodes are different in BHJ and BL devices, the transport of charges is thermally activated in most of the OSCs and should be 0 at 0 K. Therefore, one would expect the V_{OC}^0 to be the same for BL and BHJ devices made of the same materials if the effective bandgap remains the same in both device architectures.

In this study, we compare the temperature-dependent J - V characteristics of planar BL and BHJ OSCs based on NFA (ITIC) and fullerene (PC₇₁BM) acceptors and find that while the derived values of V_{OC}^0 are equivalent for BL and BHJ PC₇₁BM-based cells, this is not the case for the studied BL and BHJ ITIC-based cells. Such a counterintuitive observation indicates energy-level changes from the neat to the blend form of the same materials. The morphological changes of NFA,

namely ITIC, observed in grazing incidence wide-angle X-ray scattering (GIWAXS) measurements provide an explanation for the energy-level differences. The findings of this study suggest that the changes in the energy levels of NFA materials in blends compared to their neat forms can be significant enough to lead to V_{OC} changes for certain NFA based BHJ devices, and thus need to be carefully addressed when studying the effect of energetic level offset on device operations of OSCs.

2. Results

Three different material systems have been investigated in inverted BHJ devices covering polymer:fullerene (PTB7-Th:PC₇₁BM)^[27] and polymer:NFA (PTB7-Th:ITIC,^[28] J52:ITIC^[29]) systems. The chemical structures of the materials used are shown in **Figure 1a**. The same donor PTB7-Th was paired with PC₇₁BM and ITIC to investigate the potential difference between the acceptors, and two donor materials (PTB7-Th and J52) were paired with ITIC to examine the influence of donor materials. The BL devices were prepared by first spin-coating the acceptor layer onto the device substrate and then laminating a layer of neat donor polymer on top (see Experimental Section for more details). The light and dark J - V curves of BHJ and BL cells based on these pairings are shown in **Figure 1b**, with the photovoltaic parameters presented in **Table 1**. As shown in **Figure 1b** and **Table 1**, the comparison of the BHJ and BL devices reveals the difference between fullerene and NFA-based systems. For PTB7-Th:PC₇₁BM, the BL device has a significantly lower V_{OC} and J_{SC} . Such a change is not surprising, because the efficiency of charge separation is expected to be much less in BL devices

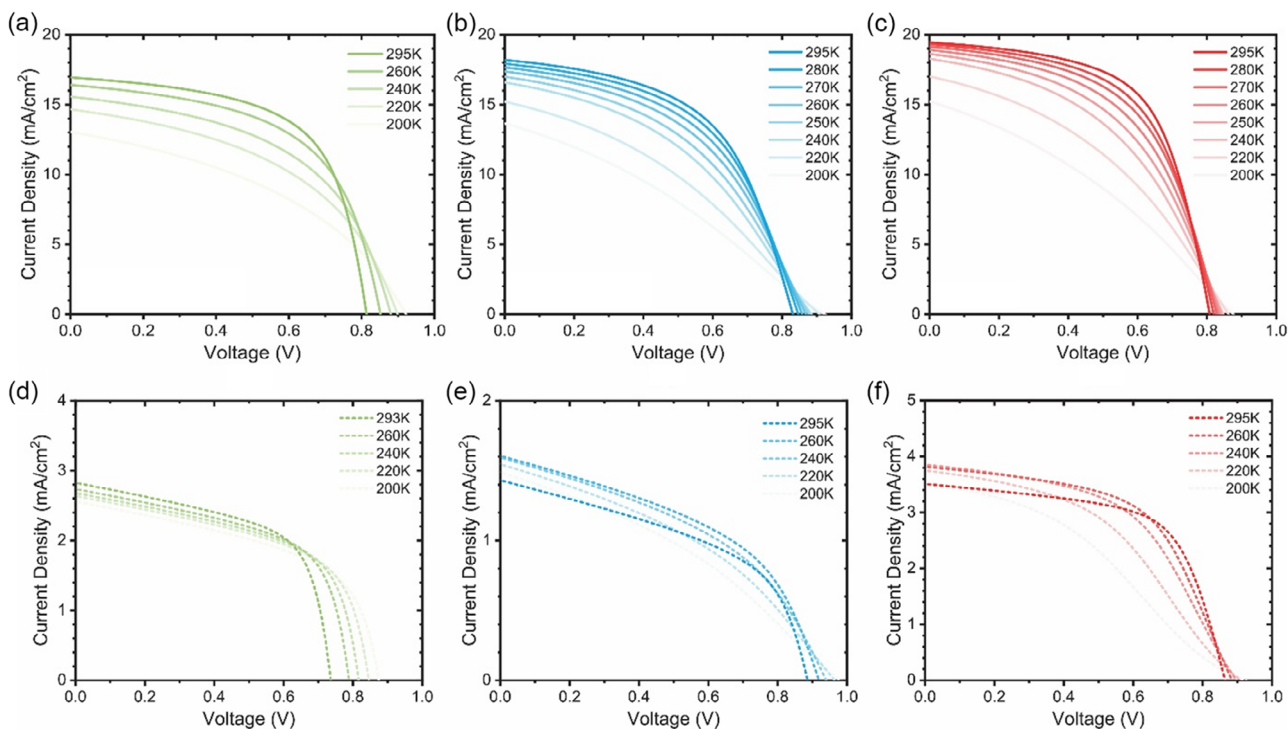


Figure 2. a–c) Temperature-dependent J - V characteristics of BHJ devices of a) PTB7-Th:PC₇₁BM, b) PTB7-Th:ITIC, and c) J52:ITIC. d–f) Temperature-dependent J - V characteristics of bilayer (BL) devices of d) PTB7-Th:PC₇₁BM, e) PTB7-Th:ITIC, and f) J52:ITIC.

resulting in lower-charge-carrier densities and hence smaller quasi-Fermi-level splitting and consequently a lower V_{OC} . In contrast, both the J52:ITIC and PTB7-Th:ITIC BL show an improvement in V_{OC} compared to the corresponding BHJ devices, though the J_{SC} of the ITIC BL devices is also significantly lower than that of the BHJ devices.

To understand the different behavior of the fullerene and NFA-based systems, temperature-dependent light $J-V$ measurements of BHJ and BL devices were performed for obtaining the temperature-dependent V_{OC} , with the obtained $J-V$ curves shown in Figure 2. For all the temperature-dependent measurements, a warm white light-emitting diode (LED) was used, and the intensities were chosen so that the J_{SC} values are similar to that measured under 1 sun illumination. Within the temperature range of 200–295 K, all BHJ and BL devices function reliably during temperature-dependent measurements, as shown by the $J-V$ curves in Figure 2. The J52/ITIC BL device shown in Figure 2f has a slightly S-shaped curve at 200 K, which is likely related to reduced mobility at low temperatures. Since the focus of this work is the temperature dependence of V_{OC} , the V_{OC} values of all devices were extracted from these light $J-V$ curves and

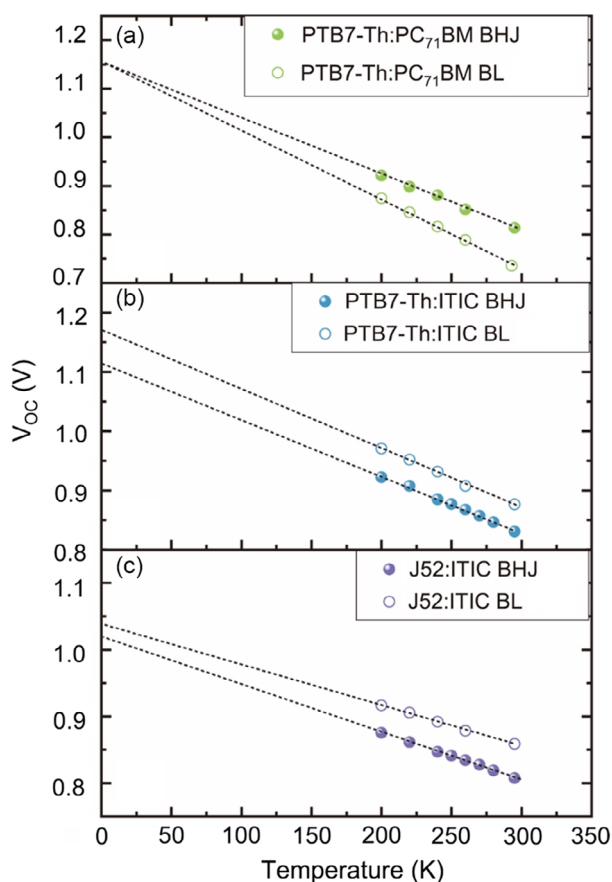


Figure 3. Comparison of temperature-dependent open-circuit voltage (V_{OC}) curves of BHJ and BL devices made of the same materials: a) PTB7-Th: PC₇₁BM, b) PTB7-Th:ITIC, and c) J52:ITIC. The values of V_{OC}^0 were obtained through linear extrapolation to temperature-dependent V_{OC} curves to 0 K. The obtained values for each system are summarized in Table 1.

plotted as a function of temperature in Figure 3. As shown in Figure 3, the V_{OC} of all the devices measured exhibits a monotonic and linear increase with decreasing temperature within the temperature range of 200–295 K. V_{OC} turnover was not observed within this temperature range, indicating that V_{OC} is not affected by the leakage current.^[30]

Linear fitting of the V_{OC} versus T curves was then conducted, with the obtained values of V_{OC}^0 determined via extrapolation of V_{OC} to 0 K summarized in Table 2. As shown in Figure 3, comparing the V_{OC} value of the BL and BHJ devices made of the same materials, the ITIC-based systems show a different trend from the fullerene-based system. For the PTB7-Th:PC₇₁BM system, the BL device at room temperature shows a significantly lower V_{OC} (0.694 V) than that of the BHJ device (0.813 V). In contrast, for the two ITIC-based systems, the BL devices exhibit higher V_{OC} (> 0.05 V) than that of the corresponding BHJ devices. Extrapolating to 0 K, the values of V_{OC}^0 of the PTB7-Th:PC₇₁BM BL and PTB7-Th:PC₇₁BM BHJ device are found to be the same, while a discrepancy is seen for the ITIC-based systems. The discrepancy between the V_{OC}^0 (0.053 V) of the BHJ and BL device is close to their room-temperature V_{OC} difference (0.051 V). Therefore, their difference in room-temperature V_{OC} may be sufficiently explained by their V_{OC}^0 value difference, which suggests that this difference originates from energy-level differences, rather than from differences in the rate of bimolecular recombination in the two device architectures. For the J52:ITIC system, a difference in the V_{OC}^0 of BL and BHJ devices is also seen (difference of 0.024 V) though this difference is not enough to account for the ≈ 0.05 V difference seen at room temperature suggesting that both energy-level difference and different recombination losses contribute to the different V_{OC} observed at room temperature. To make sure that the observed discrepancies are not caused by the error of linear fitting, the ITIC-based BHJ devices were measured at different intensities, and the V_{OC} values obtained by the simultaneous linear fitting of V_{OC} versus T curves at different intensities are identical to the values shown in Table 2. The details of these fittings can be found in Figure S4, Supporting Information.

As non-fullerene small molecule acceptors such as ITIC have been reported to have different polymorphs when deposited under different conditions,^[22] GIWAXS has been performed to study the microstructure of neat materials and thin-film

Table 2. Summary of energetics obtained from the dark and light analysis of all inverted BHJ and bilayer devices. The qV_{OC}^0 and qV_{OC}^{295K} values are taken from the same device to exclude device-to-device variations. The errors quoted for these values reflect uncertainties obtained from the linear fitting.

Materials D:A	Device architecture	qV_{OC}^{295K} [eV]	qV_{OC}^0 [eV]
PTB7-Th:PC ₇₁ BM	Inverted BHJ	0.813	1.151 ± 0.006
PTB7-Th:PC ₇₁ BM	Inverted BL	0.694	1.154 ± 0.008
PTB7-Th:ITIC	Inverted BHJ	0.831	1.119 ± 0.005
PTB7-Th:ITIC	Inverted BL	0.882	1.172 ± 0.006
J52:ITIC	Inverted BHJ	0.806	1.017 ± 0.002
J52:ITIC	Inverted BL	0.864	1.041 ± 0.004

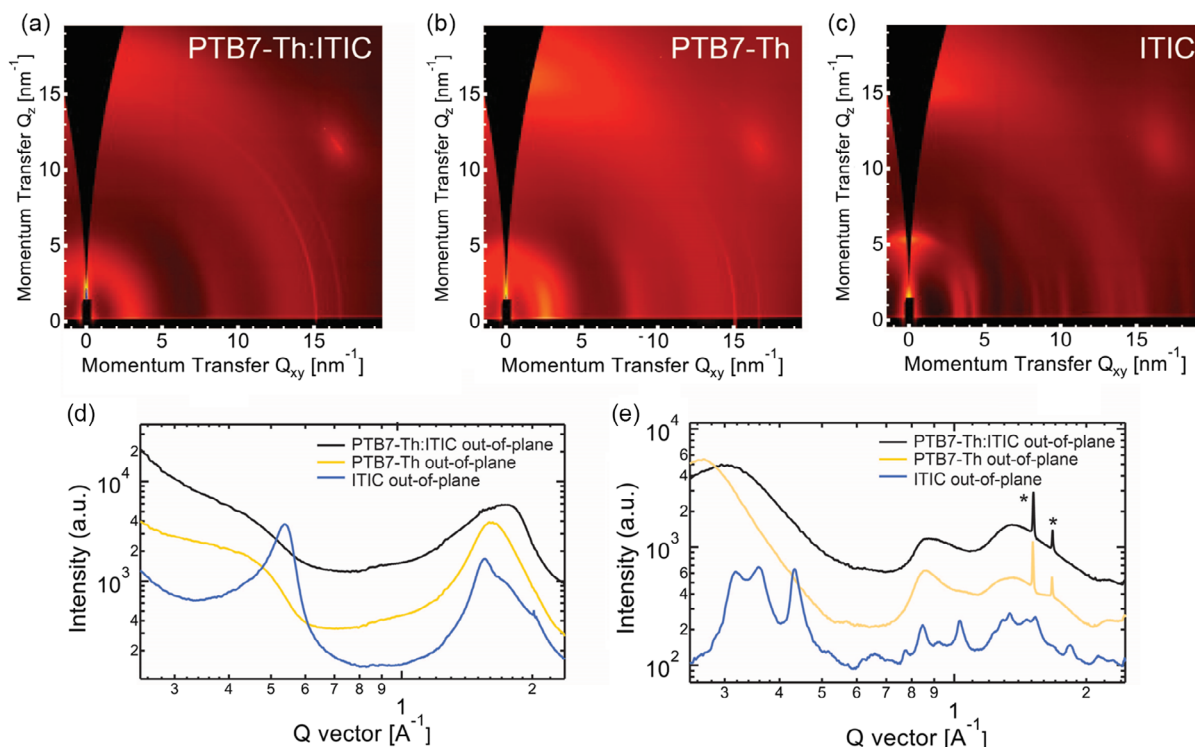


Figure 4. a–c) The 2D grazing incidence wide-angle X-ray scattering (GIWAXS) patterns of PTB7-Th:ITIC, PTB7-Th, and ITIC, respectively. d) Reduced 1D GIWAXS profiles along out-of-plane direction. e) Reduced 1D GIWAXS profiles along in-plane direction. The sharp features in the in-plane plots of PTB7-Th and PTB7-Th:ITIC in (e) labeled with asterisk symbols are artifacts likely caused by silicon dust on the sample.

blends of the PTB7-Th:ITIC system to evidence differences in molecular packing. The fabrication conditions of the films for GIWAXS measurement were kept the same as that of the BHJ devices. All the films were measured as-cast without annealing, replicating device fabrication conditions. From the 2D GIWAXS patterns shown in **Figure 4**, ITIC exhibits multiple sharp diffraction peaks along the in-plane direction in the neat film, along with pronounced out-of-plane peaks at $Q = 0.55 \text{ \AA}^{-1}$ and $Q = 1.55 \text{ \AA}^{-1}$. The scattering pattern of neat ITIC is consistent with the “Phase I” polymorph as characterized by Marina et al.^[22] These crystalline scattering features of neat ITIC however are not seen in the blend film, which is devoid of any diffraction features characteristic of ITIC, indicating that the crystallization of ITIC is suppressed when blended with PTB7-Th. Suppression of ITIC crystallinity is also seen in the blend with J52 (see Figure S3, Supporting Information). Thus, compared to neat ITIC, which adopts a well-defined crystalline polymorph, in the blends with PTB7-Th and J52 ITIC exhibits a rather disordered packing.

3. Discussion

For the PC₇₁BM-based devices, the BL device has a lower V_{OC} at room temperature compared to the BHJ device. As V_{OC} is influenced by energetic as well as kinetic factors at room temperature, the lower V_{OC} of the PC₇₁BM BL device can be understood in terms of a lower-charge-generation rate (the BL device has a reduced interfacial area) and/or a faster recombination rate.

The V_{OC}^0 of the BL and BHJ PC₇₁BM devices however are the same, indicating that when kinetic factors are excluded, the V_{OC} (as influenced by energetics) of these two devices are the same.

For the NFA-based devices, the room-temperature V_{OC} of the BL devices is higher than that of the corresponding BHJ devices. Such a situation is not easy to explain in terms of differences in kinetics. The V_{OC}^0 of the NFA BL devices are also higher, which provides strong evidence that the differences in V_{OC} at room temperature are indeed the result of differences in the energetics of the BL and BHJ NFA cells. Differences in microstructure evidenced by GIWAXS provide an explanation as to why the BL and BHJ devices based on ITIC have different V_{OC}^0 . The fact that PC₇₁BM is a relatively isotropic molecule and does not have the same complicated crystalline behavior as ITIC provides an explanation as to why the energetics of PC₇₁BM are essentially the same in the neat film as in the blend. In this case, the energy levels (LUMO of PC₇₁BM and HOMO of PTB7-Th) are less likely to change from neat films to blends.

For NFAs with richer microstructure and stronger connections between molecular packing and energetics, the V_{OC}^0 discrepancies observed here between BL and BHJ devices indicate that care needs to be taken when deriving LUMO values from neat samples and applying them to BHJ films. Deriving the effective bandgap for a BHJ device on the basis of the LUMO measured for neat ITIC is likely to be incorrect. Furthermore, if the LUMO (HOMO) offset is calculated from measurement of neat donor and acceptor materials, one may

conclude that the “driving force” for electron (hole) transfer is smaller than it actually is. For studies focused on systems with small driving force, LUMO (HOMO) offset ranging from negligible to 0.3 eV is often involved,^[1,8,31] which means that around 0.06 eV difference (as observed for PTB7-Th:ITIC in this study) may lead to a > 20% discrepancy of the energetic offset.

4. Conclusion

We have systematically compared the BHJ and BL devices in terms of their V_{OC}^0 , which fulfills the role as an effective bandgap of the donor:acceptor systems. The V_{OC}^0 values of BHJ and BL devices are found to be equal for PTB7-Th:PC₇₁BM system, but different for ITIC-based systems. The discrepancy was explained by the different molecular packing of ITIC in neat films compared to in blends, which can bring about changes in energetic levels of the corresponding donor:acceptor interfaces, leading to different V_{OC}^0 values. As we measure different V_{OC}^0 values for BHJ and BL devices, care must be taken when deriving energy-level offsets from neat films for comparison with the V_{OC} values of BHJ blends, especially for those based on non-fullerene molecules which have more complicated microstructure behavior compared to PC₇₁BM.

5. Experimental Section

Materials: ITIC was synthesized in-house according to previous reports.^[32] PTB7-Th (YY16042CH) and J52 were purchased from 1-Material Inc. PC₇₁BM (TC161027) was purchased from Nano-C.

Device Fabrication: For all inverted BHJ OSCs reported in this work, a device architecture of indium tin oxide (ITO)/polyethylenimine (PEIE)/active layer/MoO_x/Ag was used. The PEIE layer was spin-coated at 5000 rpm using 0.4 wt% solution in 2-methoxyethanol and was annealed at 120 °C under ambient conditions. The deposition conditions of the active layer of inverted BHJ devices are presented in Supporting Information. After spin-coating of the active layer, a 12 nm layer of MoO_x and a 100 nm of Ag were then deposited by thermal evaporation in a vacuum evaporator (Angstrom Engineering). Devices for low-temperature characterization were not encapsulated and were transferred into a vacuum chamber of the cryostat for measurement. Devices for room-temperature characterization only were encapsulated using epoxy resin (Devcon 2-Ton) with a top glass slide.

For inverted BL devices, fabrication followed in the same manner except that the active layer was replaced with a BL. The acceptor was spin-coated directly onto the PEIE modified ITO substrate first. The donor layer was spin-coated on a clean and oxygen plasma-treated glass slide and then floated off onto deionized water. The acceptor-coated substrate was then lowered onto the floating donor layer and picked up with tweezers. For neat layers used in BLs, PTB7-Th was dissolved in chlorobenzene (10 mg mL⁻¹) and spin-coated at 3000 rpm. PC₇₁BM was dissolved in chlorobenzene (20 mg mL⁻¹) and spin-coated at 4000 rpm. ITIC was dissolved in chlorobenzene (20 mg mL⁻¹) and spin-coated at 2000 rpm. The thickness of each layer was around 50 nm as measured by a Dektak 150 surface profilometer.

Temperature-Dependent Measurement: All temperature-dependent measurements were conducted under vacuum using a continuous flow cryostat (Janis Research Model ST-100 Supertran system), which had a temperature controller (Lakeshore 325) for maintaining the temperature at a set point. Before cooling down, the devices were measured at room temperature to check the device quality. After that, the cryostat sample holder was cooled down to 78 K and kept at this temperature for around 2 h to ensure that the devices were at thermal equilibrium with the sample

holder. Measurement was then taken at 78 K and the temperature was then raised by 20 K (or 10 K) at a time. After increasing the temperature, approximately 1 h was allowed for the device to reach thermal equilibrium before the next measurement was taken. The current–voltage curves were recorded using a Keithley 2400 model source–measure unit for all temperature-dependent measurements.

GIWAXS: GIWAXS measurements were performed at the small angle X-ray scattering (SAXS)/wide angle X-ray scattering (WAXS) beamline at the Australian Synchrotron.^[33] Samples were prepared as per devices using bare silicon wafers as substrates. A photon energy of 15 keV was used with a sample detector distance of 67.2 mm calibrated using a silver behenate standard. An in-vacuum Dectris Pilatus 2 M detector was used with the entire beam path placed in vacuum to remove background scattering from air and X-Ray windows. The scattering patterns were measured as a function of incident angle. The data shown were acquired with an angle of incidence near the critical angle (typically around 0.1°) that maximized scattering intensity from the sample. Data reduction and analysis were performed using an altered version of the NIKA analysis package^[34] implemented in Igor Pro.

Supporting Information

Supporting Information is available from the Wiley Online Library or from the author.

Acknowledgements

This work was performed in part at the SAXS/WAXS beamline at the Australian Synchrotron, part of ANSTO. Mr. Hao Liu is acknowledged for his assistance with sample preparation for GIWAXS measurements.

Open access publishing facilitated by Monash University, as part of the Wiley - Monash University agreement via the Council of Australian University Librarians.

Conflict of Interest

The authors declare no conflict of interest.

Data Availability Statement

The data that support the findings of this study are available from the corresponding author upon reasonable request.

Keywords

energy loss, non-fullerene acceptors, organic solar cells, small energetic offset, temperature-dependent measurements

Received: June 21, 2023

Revised: August 9, 2023

Published online:

- [1] A. Classen, C. L. Chochos, L. Lürer, V. G. Gregoriou, J. Wortmann, A. Osvet, K. Forberich, I. McCulloch, T. Heumüller, C. J. Brabec, *Nat. Energy* **2020**, *5*, 711.
- [2] N. Gasparini, F. V. A. Camargo, S. Frühwald, T. Nagahara, A. Classen, S. Roland, A. Wadsworth, V. G. Gregoriou, C. L. Chochos, D. Neher, M. Salvador, D. Baran, I. McCulloch, A. Görling, L. Lürer, G. Cerullo, C. J. Brabec, *Nat. Commun.* **2021**, *12*, 1772.

- [3] K. D. Rosenthal, M. P. Hughes, B. R. Luginbuhl, N. A. Ran, A. Karki, S. Ko, *Adv. Energy Mater.* **2019**, *9*, 1901077.
- [4] V. Lami, A. Weu, J. Zhang, Y. Chen, Z. Fei, M. Heeney, R. H. Friend, Y. Vaynzof, *Joule* **2019**, *3*, 2513.
- [5] F. Jin, J. Yuan, W. Guo, Y. Xu, Y. Zhang, C. Sheng, W. Ma, H. Zhao, F. Jin, W. P. Guo, H. B. Zhao, J. Y. Yuan, Y. L. Xu, Y. N. Zhang, W. L. Ma, C. X. Sheng, *Adv. Funct. Mater.* **2018**, *28*, 1801611.
- [6] S. Li, L. Zhan, C. Sun, H. Zhu, G. Zhou, W. Yang, M. Shi, C. Z. Li, J. Hou, Y. Li, H. Chen, *J. Am. Chem. Soc.* **2019**, *141*, 3073.
- [7] S. Chen, Y. Wang, L. Zhang, J. Zhao, Y. Chen, D. Zhu, H. Yao, G. Zhang, W. Ma, R. H. Friend, P. C. Y. Chow, F. Gao, H. Yan, *Adv. Mater.* **2018**, *30*, 1804215.
- [8] C. Sun, S. Qin, R. Wang, S. Chen, F. Pan, B. Qiu, Z. Shang, L. Meng, C. Zhang, M. Xiao, C. Yang, Y. Li, *J. Am. Chem. Soc.* **2020**, *142*, 1465.
- [9] S. Karuthedath, J. Gorenflot, Y. Firdaus, N. Chaturvedi, C. S. P. De Castro, G. T. Harrison, J. I. Khan, A. Markina, A. H. Balawi, T. A. Dela Peña, W. Liu, R.-Z. Liang, A. Sharma, S. H. K. Paleti, W. Zhang, Y. Lin, E. Alarousu, D. H. Anjum, P. M. Beaujuge, S. De Wolf, I. McCulloch, T. D. Anthopoulos, D. Baran, D. Andrienko, F. Laquai, *Nat. Mater.* **2020**, *20*, 378.
- [10] K. Nakano, *Nat. Commun.* **2019**, *10*, 2520.
- [11] S. D. Collins, C. M. Proctor, N. A. Ran, T.-Q. Nguyen, *Adv. Energy Mater.* **2016**, *6*, 1501721.
- [12] A. Armin, I. Kassal, P. E. Shaw, M. Hamsch, M. Stolterfoht, D. M. Lyons, J. Li, Z. Shi, P. L. Burn, P. Meredith, *J. Am. Chem. Soc.* **2014**, *136*, 11465.
- [13] J. Brandt, J. Han, C. S. P. De Castro, E. Yengel, J. Gorenflot, T. Anthopoulos, F. Laquai, A. Sharma, D. Baran, J. Brandt, J. Han, C. S. P. De Castro, E. Yengel, J. Gorenflot, T. Anthopoulos, F. Laquai, A. Sharma, D. Baran, *Adv. Mater.* **2022**, *34*, 2202575.
- [14] X. Li, Q. Zhang, J. Yu, Y. Xu, R. Zhang, C. Wang, H. Zhang, S. Fabiano, X. Liu, J. Hou, F. Gao, M. Fahlman, *Nat. Commun.* **2022**, *13*, 2046.
- [15] D. C. Coffey, B. W. Larson, A. W. Hains, J. B. Whitaker, N. Kopidakis, O. V. Boltalina, S. H. Strauss, G. Rumbles, *J. Phys. Chem. C* **2012**, *116*, 8916.
- [16] M. C. Scharber, D. Mühlbacher, M. Koppe, P. Denk, C. Waldauf, A. J. Heeger, C. J. Brabec, *Adv. Mater.* **2006**, *18*, 789.
- [17] C. Yang, J. Zhang, N. Liang, H. Yao, Z. Wei, C. He, X. Yuan, J. Hou, *J. Mater. Chem. A* **2019**, *7*, 18889.
- [18] L. J. A. Koster, E. C. P. Smits, V. D. Mihailetchi, P. W. M. Blom, *Phys. Rev. B* **2005**, *72*, 085205.
- [19] W. Li, M. Chen, J. Cai, E. L. K. Spooner, H. Zhang, R. S. Gurney, D. Liu, Z. Xiao, D. G. Lidzey, L. Ding, T. Wang, *Joule* **2019**, *3*, 819.
- [20] L. Ye, K. Weng, J. Xu, X. Du, S. Chandrabose, K. Chen, J. Zhou, G. Han, S. Tan, Z. Xie, Y. Yi, N. Li, F. Liu, J. M. Hodgkiss, C. J. Brabec, Y. Sun, *Nat. Commun.* **2020**, *11*, 6005.
- [21] G. Zhang, X. K. Chen, J. Xiao, P. C. Y. Chow, M. Ren, G. Kupgan, X. Jiao, C. C. S. Chan, X. Du, R. Xia, Z. Chen, J. Yuan, Y. Zhang, S. Zhang, Y. Liu, Y. Zou, H. Yan, K. S. Wong, V. Coropceanu, N. Li, C. J. Brabec, J. L. Bredas, H. L. Yip, Y. Cao, *Nat. Commun.* **2020**, *11*, 3943.
- [22] S. Marina, A. D. Scaccabarozzi, E. Gutierrez-Fernandez, E. Solano, A. Khirbat, L. Ciamparuchi, A. Iturrospe, A. Balzer, L. Yu, E. Gabirondo, X. Monnier, H. Sardon, T. D. Anthopoulos, M. Caironi, M. Campoy-Quiles, C. Müller, D. Cangialosi, N. Stingelin, J. Martin, *Adv. Funct. Mater.* **2021**, *31*, 2103784.
- [23] B. Kitchen, O. Awartani, R. J. Kline, T. McAfee, H. Ade, B. T. O'Connor, *ACS Appl. Mater. Interfaces* **2015**, *7*, 13208.
- [24] K. Vandewal, K. Tvingstedt, A. Gadisa, O. Inganäs, J. V. Manca, *Phys. Rev. B* **2010**, *81*, 125204.
- [25] U. Rau, *Phys. Rev. B* **2007**, *76*, 085303.
- [26] U. Hörmann, J. Kraus, M. Gruber, C. Schuhmair, T. Linderl, S. Grob, S. Kapfinger, K. Klein, M. Stutzman, H. J. Krenner, W. Brütting, *Phys. Rev. B* **2013**, *88*, 235307.
- [27] W. Huang, E. Gann, L. Thomsen, C. Dong, Y. B. Cheng, C. R. McNeill, *Adv. Energy Mater.* **2015**, *5*, 1401259.
- [28] X. Wang, Y. Yang, Z. He, H. Wu, Y. Cao, *J. Mater. Chem. C* **2019**, *7*, 14861.
- [29] H. Bin, Z. G. Zhang, L. Gao, S. Chen, L. Zhong, L. Xue, C. Yang, Y. Li, *J. Am. Chem. Soc.* **2016**, *138*, 4657.
- [30] Y. Tang, J. M. Bjuggren, Z. Fei, M. R. Andersson, M. Heeney, C. R. McNeill, *Sol. RRL* **2020**, *4*, 2000375.
- [31] M. S. Niu, K. W. Wang, X. Y. Yang, P. Q. Bi, K. N. Zhang, X. J. Feng, F. Chen, W. Qin, J. L. Xia, X. T. Hao, *J. Phys. Chem. Lett.* **2019**, *10*, 7100.
- [32] Y. Lin, J. Wang, Z. G. Zhang, H. Bai, Y. Li, D. Zhu, X. Zhan, *Adv. Mater.* **2015**, *27*, 1170.
- [33] N. M. Kirby, S. T. Mudie, A. M. Hawley, D. J. Cookson, H. D. T. Mertens, N. Cowieson, V. Samardzic-Boban, *J. Appl. Crystallogr.* **2013**, *46*, 1670.
- [34] J. Ilavsky, *J. Appl. Crystallogr.* **2012**, *45*, 324.